Investigating surface visco-elasticity in a thermally driven 2D microfoam

Vincent Miralles[1], Emmanuelle Rio[2], Isabelle Cantat[3], and Marie-Caroline Jullien[1]
[1]*MMN, UMR CNRS Gulliver 7083, PSL research University, ESPCI ParisTech, 10 rue Vauquelin, F-75005 Paris, France*
[2]*Laboratoire de Physique des Solides, UMR CNRS & Université Paris-Sud 8502, 91405 Orsay Cedex, France*
[3]*IPR, UMR CNRS 6251, Universite de Rennes 1, 35000 Rennes, France*
(Dated: June 19, 2016)

SURFACE TENSION MEASUREMENTS

DOH concentration dependence

Since the adsorption/desorption process of both SDS and DOH are involved in the stabilisation of the air-water interface [1–7], we measured the time evolution of the surface tension for different DOH bulk concentrations at constant SDS concentration (2 CMC), using the rising bubble technique [8] at constant temperature T=25 °C.

The experiments presented in Fig.1 were performed at a constant bubble volume equal to $V_b = 8.0\ \mu$L in the rising bubble geometry. The finest time resolution used at short times in the experiments presented in Fig.1 is equal to 4 ms. When the air-water interface is only stabilised by SDS (*i.e.* [DOH] = 0), the surface tension does not evolve with time ($\gamma_0 = 38.5$ mN.m^{-1}), which means that the characteristic adsorption time for SDS at 2 CMC is shorter than 4 ms. Hence we observe that the value of the surface tension at equilibrium decreases when increasing the DOH bulk concentration (see Fig.1), which gives access to the evolution of γ_{eq} with the DOH bulk concentration (see Fig.2):

$$\frac{\partial \gamma_{eq}}{\partial c} = -1.00\,\mathrm{N.m^2.mol^{-1}} \qquad (1)$$

Temperature dependence

Since the surface tension depends on temperature, we coupled a thermal bath with a Wilhelmy plate to characterise the evolution of $\partial_T \gamma$ as a function of the DOH bulk concentration. Fig.3 shows that the dependence of the surface tension as a function of the temperature is fairly independent of the DOH concentration, leading to:

$$\frac{\partial \gamma}{\partial T} = -2.1\,10^{-4}\,\mathrm{N.m^{-1}.K^{-1}} \qquad (2)$$

LANGMUIR-VON SZYSZKOWSKI ISOTHERM

Since DOH is an insoluble surfactant presenting a localised adsorption and no interaction with SDS [3, 4],

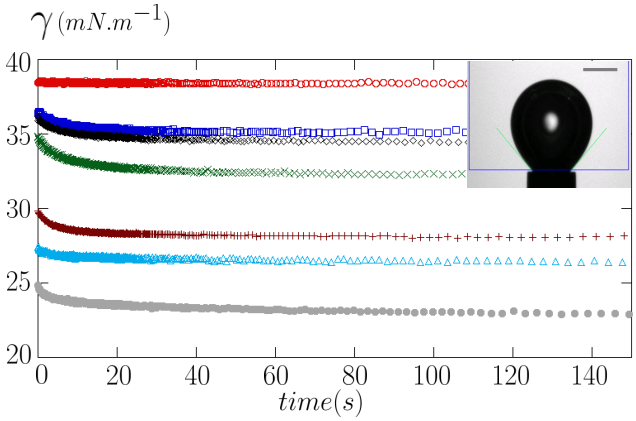

FIG. 1. Time evolution of the surface tension for a liquid phase consisting of SDS at 2 CMC and DOH respectively at: 0 mol.L^{-1} (open circles), 8.0 10^{-7} mol.L^{-1} (open squares), 1.6 10^{-6} mol.L^{-1} (open diamonds), 3.2 10^{-6} mol.L^{-1} (crosses), 6.4 10^{-6} mol.L^{-1} (plus signs), 9.6 10^{-6} mol.L^{-1} (open triangles) and 1.3 10^{-5} mol.L^{-1} (solid circles). Inset: Snapshot showing the rising bubble experiment. The scalebar represents 1.00 mm.

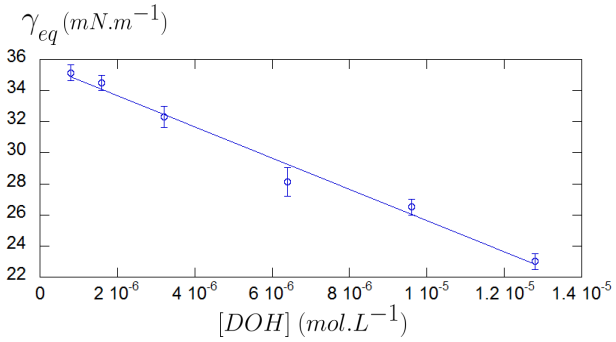

FIG. 2. Equilibrium surface tension as a function of DOH bulk concentration. The solid blue line is the best linear fit.

we assume that the DOH surface concentration at the air-water interface ($\Gamma(c)$) follows Langmuir's adsorption kinetics:

$$\frac{\Gamma(c)}{\Gamma_\infty} = \frac{Kc}{1+Kc} \qquad (3)$$

where Γ_∞ and K are respectively the maximum surface excess and the Von Szyszkowski constant [9–12], which will be estimated in the following. Hence the Gibbs-Duhem relation [13] links the variation of surface tension

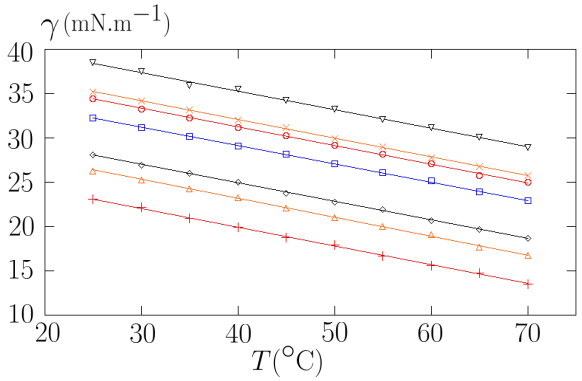

FIG. 3. Evolution of the surface tension as a function of the temperature for water phases consisting of SDS at 2CMC and DOH at 0 mol.L^{-1} (inverted triangles), 8.0 10^{-7} mol.L^{-1} (crosses), 1.6 10^{-6} mol.L^{-1} (circles), 3.2 10^{-6} mol.L^{-1} (squares), 6.4 10^{-6} mol.L^{-1} (diamonds), 9.6 10^{-6} mol.L^{-1} (triangles) and 1.3 10^{-5} mol.L^{-1} (plus signs). Solid lines correspond to a linear fit for each dataset.

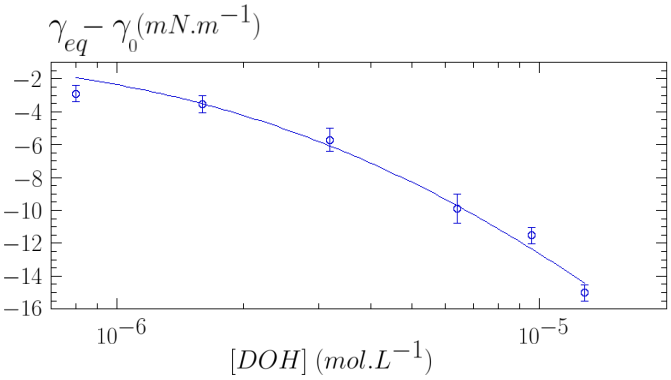

FIG. 4. $\gamma_{eq} - \gamma_0$ as a function of DOH bulk concentration (logscale). The solid blue line is the best fit obtained from the Langmuir-Von Szyszkowski isotherm (Eq.5).

to the variation of chemical potentials (μ_i) for all the chemicals (index i) in presence: $\mathrm{d}\gamma = -\sum_i \Gamma_i\, \mathrm{d}\mu_i$. Since the SDS concentration is a constant in all the experiments performed, only the variation of chemical potential for DOH has to be taken into account:

$$\mathrm{d}\gamma = -\Gamma \mathrm{d}\mu_{DOH} \tag{4}$$

Integrating Eq.4 leads to the Langmuir-Von Szyszkowski isotherm:

$$\gamma_{eq}(c) - \gamma_0 = -\Gamma_\infty \mathcal{R}T \ln(1 + Kc) \tag{5}$$

where $\mathcal{R} = 8.31$ J.mol^{-1}.K^{-1} is the ideal gas constant and T = 298 K is the absolute temperature, taken constant in all the experiments carried on in this section. Fitting the values of K and Γ_∞ from the experimental data leads to: $K = 2.86\,(\pm 0.30)\ 10^5$ L.mol^{-1} and $\Gamma_\infty = 5.53\,(\pm 3.12)\ 10^{-6}$ mol.m^{-2}, see Fig.4. The maximum interfacial coverage ω_∞ can thus be estimated from the value of Γ_∞:

$$\omega_\infty = \frac{1}{\mathcal{N}_a\, \Gamma_\infty} \tag{6}$$

where $\mathcal{N}_a = 6.02\ \ 10^{23}$ mol^{-1} is the Avogadro constant. We find $\omega_\infty = 30.3$ Å^2/molecule with lower and upper bounds respectively equal to 19.3 and 70.4 Å^2/molecule, taking into account the incertitude on Γ_∞. These values are consistent with the literature [13].

ELASTIC BEHAVIOUR EVIDENCE

This section brings to light the elastic behaviour of the air-water interface when stabilised by DOH molecules [14–17]. For an insoluble monolayer like the one created by DOH molecules at the air-water interface, the *Gibbs-Marangoni elastic modulus* (E_{GM}) writes [13, 18]:

$$E_{GM} = +\frac{\mathrm{d}\gamma}{\mathrm{d}\ln A} = -\frac{\mathrm{d}\gamma}{\mathrm{d}\ln \Gamma} \tag{7}$$

where A is the area considered. Here we carried on bubble volume cycles to get insight in the elastic behaviour of the air-water interface in two cases, corresponding to an interface stabilised by *(i)* SDS at 2 CMC on its own, and *(ii)* SDS at 2 CMC together with DOH at $3.2\,10^{-6}$ mol.L^{-1}, see Fig.5. For both experiments, we performed 5 cycles of 5 s-period, for a volume variation amplitude set to $\Delta V_b/V_b$= 12.5 %.

Fig.5-a shows that for an interface stabilised by SDS only, the surface tension is not altered by the volume variation, which means that the adsorption-desorption kinetics of the SDS molecules at the interface is much faster than the characteristic time of the applied stress. This qualitative observation is consistent with the fact that r is always equal to zero in that case, independently of the value of e/R.

Fig.5-b corresponds to an interface stabilised by both SDS and DOH. First we wait for the surface tension to reach its equilibrium value before applying the volume variation cycles. Results show that a surface tension variation goes along with a volume variation, going in the same direction. This means that for a compression of the interface (*i.e.* a decrease in V_b), the number of DOH molecules adsorbed per unit area increases, leading to a decrease in surface tension. Similarly, a dilation of the interface (*i.e.* an increase in V_b) translates into a decrease in the number of DOH molecules adsorbed per unit area, leading to an increase in surface tension. Finally, these measurements shed light on the qualitative elastic behaviour of an air-water interface stabilised by both SDS and DOH, in the range of concentrations considered hereby.

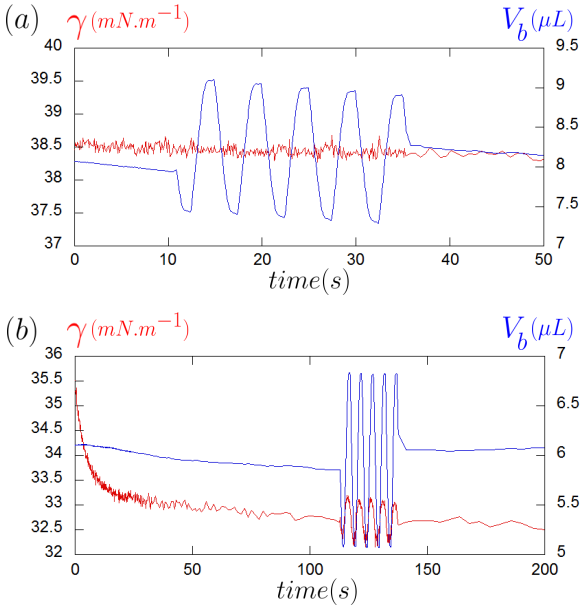

FIG. 5. Surface tension (in red) and bubble volume (in blue) as a function of time for a liquid phase consisting of SDS at 2 CMC and DOH respectively at 0 mol.L^{-1} for (a) and 3.2 10^{-6} mol.L^{-1} for (b).

ADDITIONNAL MODELS FOR THE GIBBS ELASTICITY CONTRIBUTION

• Model 2: diffusion across the film.

The first scaling law proposed for the diffusion field was based on the assumption of diffusion along the shortest line between bubbles 1 and 2. Here we assume in contrast that the surfactants diffuse across the thinnest layer of solution. In our confined geometry, below a critical liquid fraction, the bubbles are deformed by the presence of the others. This leads to the formation of thin films between bubbles, of thickness $h \sim 20$ nm set by the disjoining pressure, and of characteristic size $R \times \sqrt{eh}$ [19, 20]. These films are located at the contact between the meniscii touching respectively the top and bottom plates. As their vertical extension $\sqrt{eh}$ is very small, they have been neglected in the modeling of the thermocapillary drainage. However, as their thickness is also very small, they may be relevant for the diffusion process. Here we thus write that the surfactants accumulate at the surface of the meniscii at the front of a bubble (*i.e.* meniscii almost perpendicular to the flow), and that they diffuse from bubble 1 to bubble 2 across the section $R \times \sqrt{eh}$, with a concentration gradient scaling as $\Delta c/h$. Hence the diffusive flux writes $\Phi_{\rm diff}^{1\to 2} \sim D_{\rm DOH} R \Delta c \sqrt{e/h}$, see Fig.6.c. Still considering that the system is in a steady-state at all time, the equality between the diffusive flux and the convective flux $\Phi^1_{\rm conv} \sim (\Gamma U_s)e$ leads to:

$$r_{D,2}^{th} \sim \frac{\alpha_0 \Gamma_\infty \sqrt{h} \left|\frac{\partial \gamma_{\rm eq}}{\partial c}\right|}{\eta D_{\rm DOH}} \times \frac{Kc}{1+Kc} \times \frac{e^{3/2}}{R^2} \sim 0.45 \times \frac{Kc}{1+Kc} \times \frac{e^{3/2}}{R^2} \tag{8}$$

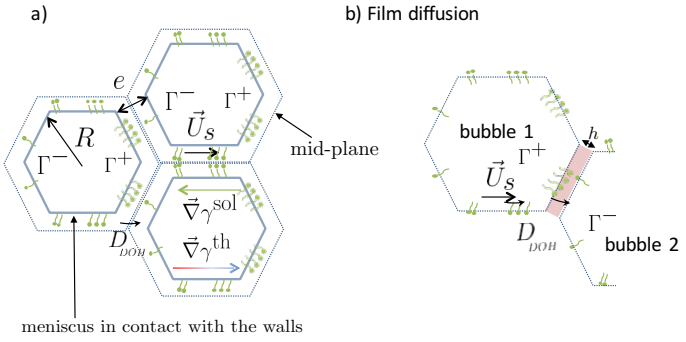

FIG. 6. a) Sketch representing the solutocapillary stress induced by the DOH molecules. *pPb* refers to the pseudo-Plateau borders [21]. b) diffusion of surfactant across the films.

Fig.7 represents the damping factor r as a function of $(Kc/1+Kc) \times e^{3/2}/R^2$. The linear fits evidenced by the solid and dashed lines in Fig.7 lead to prefactors ranging from 2.34 up to 6.45, which can be considered correct; however, it is clear that a linear fit does not reproduce the general trend of the curves as they exhibit an intercept. This intercept could be attributed to the effect of the surface shear viscosity, since $e^{3/2}/R^2 \to 0$ corresponds to $R \to \infty$. However, as in the case depicted in section 4.3 of main paper, the value of the intercept increases with e for a given DOH concentration, which is not relevant with the scaling found for Bq^s (main text, $r_{sh}^{th} \sim \frac{\epsilon}{\eta e}$).

• Model 3: convection across the meniscus

The last transport mechanism one may envision is a convective transport across the meniscus. In this configuration, the convective flux along the interface $\phi^1_{\rm conv} \sim \Gamma U_s e$ is equilibrated by the convective flux across the meniscus $\phi^{\rm vert}_{\rm conv} \sim \Delta\, c\bar{v}^{th} e^2$. Such equilibrium leads to the following scaling :

$$r_e \sim \Gamma_\infty \times \frac{\partial_c \gamma|_{\rm eq}}{\partial_T \gamma \partial_x T} \times \frac{Kc}{1+Kc} \times \frac{1}{eR} \tag{9}$$

Such scaling does not allow us to recover the experimental data as plotted on figure 7 of main text. Also, we have shown that r does not depend on the driving term $\partial_T \gamma \partial_x T$ (see Fig.5). This contribution is thus clearly negligible.

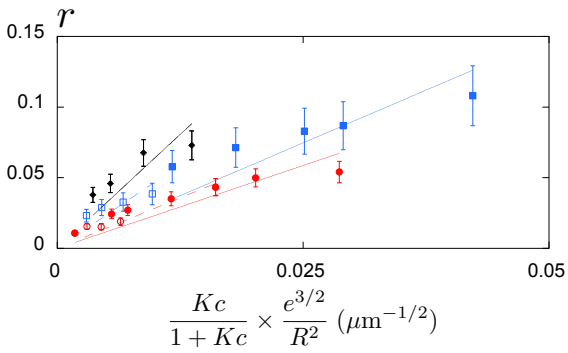

FIG. 7. Evolution of r as a function of $(Kc/1+Kc) \times e^{3/2}/R^2$ for different DOH concentrations: 1.6 10^{-6} mol.L^{-1} (circles), 3.2 10^{-6} mol.L^{-1} (squares) and 5.6 10^{-6} mol.L^{-1} (diamonds). For each dataset, the hollow (resp. solid) symbols correspond to $e = 19.3$ μm (resp. $e = 54.2$ μm). Dashed (resp. solid) lines represent the best linear fitting curves for $e = 19.3$ μm (resp. $e = 54.2$ μm), for each dataset.

[1] A. Bonfillon, F. Sicoli, and D. Langevin, Journal of colloid and interface science **168**, 497 (1994).
[2] C.-H. Chang and E. I. Franses, Colloids and Surfaces A: Physicochemical and Engineering Aspects **100**, 1 (1995).
[3] J. Fang and P. Joos, Colloids and Surfaces **65**, 113 (1992).
[4] J. Fang and P. Joos, Colloids and Surfaces **65**, 121 (1992).
[5] E. Staples, L. Thompson, I. Tucker, and J. Penfold, Langmuir **10**, 4136 (1994).
[6] H. Domínguez and M. Rivera, Langmuir **21**, 7257 (2005).
[7] J. Lu, I. Purcell, E. Lee, E. Simister, R. Thomas, A. Rennie, and J. Penfold, Journal of Colloid and Interface science **174**, 441 (1995).
[8] S.-Y. Lin, K. McKeigue, and C. Maldarelli, "Diffusion-controlled surfactant adsorption studied by pendant drop digitization," (1990).
[9] E. Chevallier, A. Mamane, H. Stone, C. Tribet, F. Lequeux, and C. Monteux, Soft Matter **7**, 7866 (2011).
[10] D. S. Valkovska and K. D. Danov, Journal of Colloid and Interface Science **223**, 314 (2000).
[11] E. Chevallier, in PhD Thesis (2013).
[12] A. Bonfillon and D. Langevin, Langmuir **9**, 2172 (1993).
[13] I. Cantat, S. Cohen-Addad, F. Elias, F. Graner, R. Höhler, O. Pitois, F. Rouyer, and A. Saint-Jalmes, Foams: structure and dynamics (Oxford University Press, 2013).
[14] L. Liggieri, F. Ravera, and M. Ferrari, Langmuir **19**, 10233 (2003).
[15] D. Vollhardt and G. Czichocki, Langmuir **6**, 317 (1990).
[16] D. Langevin, Annual Review of Fluid Mechanics **46**, 47 (2014).
[17] S. Cohen-Addad and R. Höhler, Current Opinion in Colloid & Interface Science **19**, 536 (2014).
[18] E. Lucassen-Reynders, A. Cagna, and J. Lucassen, Colloids and Surfaces A: Physicochemical and Engineering Aspects **186**, 63 (2001).
[19] C. Gay, P. Rognon, D. Reinelt, and F. Molino, The European Physical Journal E: Soft Matter and Biological Physics **34**, 1 (2011).
[20] J. Marchalot, J. Lambert, I. Cantat, P. Tabeling, and M.-C. Jullien, EPL (Europhysics Letters) **83**, 64006 (2008).
[21] V. Miralles, B. Selva, I. Cantat, and M.-C. Jullien, Physical Review Letters **112**, 238302 (2014).